# Modeling picosecond electron dynamics of pump-probe intersubband spectroscopy in *n*-type Ge/SiGe quantum wells

M. Virgilio,[1,2,*] G. Grosso,[1,2] G. Pizzi,[3,4] M. De Seta,[5] G. Capellini,[5] and M. Ortolani[6]

[1]*Dipartimento di Fisica "E. Fermi", Università di Pisa, Largo Pontecorvo 3, I-56127 Pisa, Italy*

[2]*NEST, Istituto Nanoscienze-CNR, Piazza San Silvestro 12, I-56127 Pisa, Italy*

[3]*Scuola Normale Superiore, Piazza dei Cavalieri 7, I-56126 Pisa, Italy*

[4]*Theory and Simulation of Materials, École Polytechnique Fédérale de Lausanne, Station 12, CH-1015 Lausanne, Switzerland*

[5]*Dipartimento di Fisica "E. Amaldi", Università di Roma Tre, Via Vasca Navale 84, I-00146 Roma, Italy*

[6]*Dipartimento di Fisica Sapienza, Università di Roma, Piazzale Aldo Moro 2, I-00185 Roma, Italy*

(Received 4 August 2012; revised manuscript received 23 October 2012; published 19 November 2012)

We present an energy-balance model of the electronic intersubband relaxation in optically excited *n*-type Ge/SiGe quantum wells with absorption resonance in the THz range. To this aim, the energy relaxation rates of the electron system due to interactions with both nonpolar optical and acoustic phonons are calculated. The time dependence of the relative differential transmission is also evaluated and compared with experimental data from recent pump-probe measurements. The energy relaxation rates due to acoustic and optical phonon are investigated for different electron temperatures, set by the pump beam intensity. We find that the relaxation dynamics strongly depends on the intersubband energy spacing when this is close to the optical phonon energy. Finally, our results evidence that in this material system the time dependence of the depolarization shift may have a strong influence on the relative differential transmission signal.

DOI: 10.1103/PhysRevB.86.205317 PACS number(s): 78.47.−p, 78.67.De, 73.50.Gr

## I. INTRODUCTION

Intersubband (ISB) transitions between two bound states of a quantum well (QW) have attracted great interest in the last decade, due to the development of terahertz and mid-infrared lasers and detectors based on quantum cascade designs.[1,2] Therein, the goal is to optimize parameters such as laser gain or detector responsivity by favoring the resonant interaction of photons with electrons (or holes) with respect to nonradiative carrier dynamics (e.g., electron-phonon scattering). The direct measurement of intersubband lifetimes by time-resolved pump-probe spectroscopy, together with a quantitative understanding of ISB carrier dynamics, are very important to accurately design and simulate optical devices based on ISB transitions. The large majority of studies of transient dynamics concerning ISB transitions have been carried out on single valley lattice-matched group III-V semiconductor heterostructures commonly employed in photonic devices.

ISB relaxation in narrow wells with subband separation larger than the longitudinal optical (LO) phonon energy is controlled by LO phonon emission. Subpicosecond lifetimes have been measured in agreement with theoretical estimates of the electron-phonon scattering rate.[3,4] In wide wells, where the energy spacing of the subbands is smaller than the LO phonon energy, the intersubband relaxation are predicted to be governed by acoustic phonon scattering with relaxation times of the order of a hundred picoseconds. In contrast, relaxation times ranging from few to hundreds of picoseconds have been measured[4–6] and a strong dependence on the experimental conditions and in particular on the intensity of the optical excitation has been reported. It was therefore suggested that, even if the subband separation is smaller than the LO phonon energy, electrons can relax by emitting optical phonons because of the high-energy tail of their quasiequilibrium distribution, thus giving rise to shorter relaxation times.[7,8] In this framework, it is clear that the measured relaxation time will depend on the chemical potential position and on the temperature of the electron system set by the pump event of the specific pump-probe experiment. According to the pump beam intensity and the excitation photon energy, energy relaxation by acoustic and optical phonon emission occurs at different relative rates.[8]

The main purpose of this paper is to present a theoretical model for energy relaxation after optical excitation in group IV semiconductor (Si, Ge and their alloys) quantum wells, to provide an interpretation of the results of pump-probe experiments. The lack of dipole-active optical phonons due to covalent Si-Si, Si-Ge, and Ge-Ge bonds results in qualitatively different scattering mechanisms for electrons in the excited subbands, as opposed to group III-V heterostructures with polar bonds where scattering of charge carriers by polar LO phonons is the dominant channel. The absence of dipole-active optical phonons in group IV systems offers potential advantages in the development of optoelectronic devices: nonpolar SiGe heterostructures may help fill the wavelength gap between terahertz and mid-infrared quantum cascade lasers (QCLs) and represent a viable path to increase their operation temperature. Most of time-resolved studies on the dynamics of intersubband transitions in SiGe based heterostructures have been realized on *p*-type, Si-rich structures with large band offset.[9–13] However, *n*-type structures based on strained Ge QWs (sGe) are emerging as promising alternatives because of the much simpler conduction-band structure and because of the small effective mass, in the growth direction, of electrons confined at the *L* point. Relaxation times around 30 ps for electrons in the conduction band of Ge QWs having ISB transitions in the range 15–30 meV have been measured recently by energy-degenerate pump-probe spectroscopy, where the pump and the probe beams have the same photon energy;[14] this energy can, however, be changed and tuned to the absorption

 

resonance. Although this value is considerably longer than typical values found in III-V semiconductor systems, it is much shorter than what expected if only acoustic phonons would drive the electron system back to equilibrium.[13] This fact motivates the development of an energy-balance model for the relaxation dynamics, specific for SiGe systems; this is the main result of the present work.

A complete description of ISB energy relaxation must account for many-body ($e$-$e$) interactions, which, however, occur on a much shorter time scale than electron-phonon interactions. Moreover it is known that the charge carriers in the well partially screen the incident field and thus lead to a blueshift in the absorption spectrum, named depolarization shift.[15] It is a mayor item of the present paper to address time-dependent depolarization shift effects on the THz relative differential transmission spectrum of Ge/SiGe multiple-quantum-well (MQW) systems. The magnitude of the blueshift is of the order of the effective plasma frequency of the carrier system.[15] In wide QWs with high electron density and ISB transitions in the terahertz range, this energy is comparable to the lowest ISB spacing ($E_1 - E_0$). Material systems considered in this work feature typical interacting photon energies of 12–36 meV, corresponding to radiation frequencies of 3–9 THz, and a comparable effective plasma frequency of 1–4 THz.[16] Therefore, in such systems the interplay between dynamical screening and photon absorption cross section may be observed under strong resonant ISB excitation by a monochromatic (Fourier-transform-limited) short pulse of radiation. Indeed as the ground state becomes significantly depopulated after the pump pulse, the collective screening ability of the carriers is reduced on the ultrafast time scale of electron-electron interactions[17] and this fact gives rise to dynamical detuning between the absorption resonance and the probe beam energy. In this work we demonstrate that under suitable conditions, this time-dependent detuning effects can strongly influence the relative differential transmission signals.

The paper is organized as follows: in Sec. II we introduce the investigated Ge/SiGe MQW systems. Then we present the theoretical model adopted to calculate the relaxation dynamics of the carriers and the relative differential transmission spectrum, which is the typical physical quantity measured in degenerate pump-probe experiments at different photon energies. Our results are reported in Sec. III where the coupling between electrons and acoustic/optical phonons is analyzed. The relative efficiency of the interaction with optical and acoustic phonon baths in driving the electronic system toward equilibrium is here critically discussed. In Sec. IV we address the effect of the time-dependent depolarization shift on the relative differential transmission spectra and elucidate how this effect depends on the energy detuning between the absorption resonance and the beam energy. Direct comparison of numerical data with experimental values of the relative differential transmission is also provided.

## II. SYSTEM DESCRIPTION AND METHOD

We study theoretically and numerically the Ge/SiGe MQW systems investigated experimentally in Ref. 14 by means of THz Fourier-transform spectroscopy and pump-probe degenerate spectroscopy. The considered structures were grown on Si wafers along the [001] direction, after deposition of a partially relaxed SiGe buffer layer. The in-plane lattice constant of the buffer layer corresponds to that of a relaxed $Si_{0.12}Ge_{0.88}$ alloy. The MQW samples consist of $N_{QW} = 20$ repetitions of tensile and compressive strained Ge/$Si_{0.20}Ge_{0.80}$ layers with well thickness $d_{QW}$ of 13 nm (sample S1776) or 24 nm (samples S1745 and S1750). The 30 nm thick $Si_{0.20}Ge_{0.80}$ barrier layers were doped by codeposition of phosphine with concentration $1 \times 10^{18}$ cm$^{-3}$. Doping was uniform through the complete barriers (sample S1745) or, alternatively, 10 nm thick $Si_{0.2}Ge_{0.8}$ spacers were left undoped on each side of the QWs (samples S1750 and S1776). It has been found that intersubband absorption resonances due to the $E_0 \rightarrow E_1$ transition occurs within the conduction $L$ valleys in the Ge QWs, below the optical phonon energy of Ge (37 meV), at about ~16 (15) meV for samples S1745 (S1750), and at ~ 28 meV for sample S1776. The time-dependent relative differential transmission $\Delta T/T$ due to changes of electron distribution in the two levels has been measured by degenerate pump-probe experiments at the Free Electron Laser facility FELBE[14] in Dresden, and relaxation times $\tau$ were extracted from the data by a single exponential fit with values in the range 27–33 ps. A weak temperature dependence of the relaxation time was observed up to $T = 130$ K.

To investigate theoretically the intersubband relaxation dynamics we first evaluate the MQW electronic states in the absence of any optical excitation. To this aim we rely on a multivalley effective mass model in the envelope function approximation, assuming parabolic energy valley dispersion.[18] The MQW states related to the bulk conduction minima occurring both at the $L$ point and along the $\Delta$ lines (which are at slightly higher energies) are calculated solving self-consistently the Schrödinger-Poisson equations. The model properly considers the influence of the strain fields in the well and barrier layers on the band discontinuities, the anisotropy and the tilted orientation of the mass tensors, the exchange-correlation effects in the local density approximation, the temperature dependence of the occupation probabilities, and the spatial variation of the dielectric constants. Also the incomplete ionization of the donor states associated with the $\Delta$ valleys in the barriers, which typically occurs in this kind of modulation-doped Ge/SiGe MWQ system,[18] is considered in the calculation. To this aim the Schrödinger-Poisson equations are solved iteratively, accounting for the contributions to the electrostatic potential resulting from both the ionized and bound $\Delta_2$ states in the barrier region, and from the confined carriers which populate the $L$ point QW subbands. From the self-consistent evaluation of the Fermi energy and band-edge profiles we obtain the equilibrium values $N_0$ and $N_1$ for the $L$ point two-dimensional (2D) carrier densities in the ground and first excited subbands, respectively.

As an example, we show in Fig. 1 the electronic states and the band-edge profiles calculated for the sample S1750 at $T = 4$ K. We remind that, while the four $L$ minima which are along the equivalent [111] directions remain degenerate, the six degenerate $\Delta$ valleys are split by the strain field. In particular the two conjugated $\Delta_2$ energies of the tensile strained barrier layer, located along the growth direction (red curves in Fig. 1), are pushed below the $\Delta_4$ energies (not shown

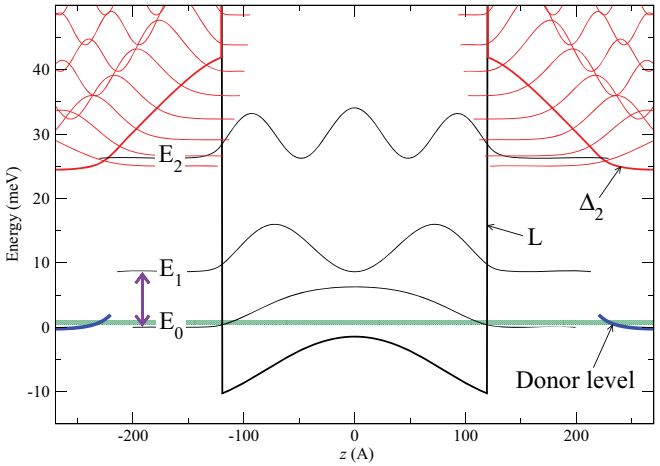


FIG. 1. (Color online) Band-edge profiles (thick lines) and squared modulus of the wave functions (thin lines) calculated for sample S1750 at $T = 4$ K in the absence of optical excitation. Band-edge profiles and states at the $L$ point (black lines, confined states $E_0$, $E_1$, and $E_2$) and at the $\Delta_2$ band edge (red lines) are displayed and marked. The donor level in the doped portion of the barrier is also represented (blue line). The green shaded area represents the energy region from the Fermi level up to $2k_BT$ above it. The violet double-tip arrow marks the $E_0 \rightarrow E_1$ transition between confined $L$ point subbands.

in Fig. 1). Moreover the bottom of the $\Delta_2$ band-edge profile is located in the barrier region where the $\Delta_2$ states are confined (see Fig. 1). As a consequence the $\Delta_2$ levels in the barriers lie in the same energy region of the excited $L$ point QW states, limiting the exploitation of the entire band-offset in device applications.[19,20] Our calculations indicate that, for the doping concentration used in the barriers, the carrier transfer from $\Delta_2$ donor states into the well region is not complete, being limited by the small energy difference between the donor level anchored to the $\Delta_2$ minima in the barrier and the $L$ point minima in the well, and by the electrostatic repulsion due to electron accumulation in the Ge layer.[18] In fact, from Fig. 1 we see that most of the donor levels (blue curve) are below the Fermi energy and then only a small fraction of the carriers are transferred into the well. For the investigated structures and in the low-temperature range, the 2D carrier densities per well resulting from the self-consistent calculations are in the 3–7 $\times$ $10^{11}$ cm$^{-2}$ range. These carrier densities are in satisfactory agreement with the values estimated experimentally from the transmission spectra (see also Ref. 18). We stress that in this range of carrier density the electronic states and the intersubband dynamics can be satisfactory described in a single-particle theoretical framework such as the one adopted in the present work.[15]

The charge imbalance in the modulation doped structures here investigated is responsible for the bending of their band-edge profile, which is apparent in in Fig. 1. In particular, the bending of the $L$ point band profile in the well region slightly reduces the energy separation between the confined $E_0$ and $E_1$ subbands with respect to the flat band condition. This transition-energy redshift contributes to suppress the emission of optical phonon during the relaxation process.

The ISB relaxation dynamics, which drives the 2D electron gas to equilibrium after optical excitation resonant with the $E_0 \rightarrow E_1$ absorption energy, is simulated by means of an energy-balance model.[7] Preliminary to the introduction of the model, we note that the presence of $\Delta_2$ states is expected to play a minor role in the relaxation dynamics of the $L$ electron gas. Indeed the $\Delta_2$ states are not populated in equilibrium conditions at low lattice temperature, and their interaction with the $L$ electrons is much weaker than the interaction between electrons in the $E_0$ and $E_1$ subbands. In fact the localization of the $L$ and $\Delta_2$ states in different spatial regions makes their overlap two orders of magnitude smaller than the one calculated for the $E_0$ and $E_1$ wave functions. The possibility of ignoring as a first approximation the presence of $\Delta_2$ states in simulating the relaxation dynamic is also supported by Ref. 14, where very similar relative differential transmission spectra and relaxation times for narrow (S1776) and wide (S1745 and S1750) MQW samples are reported, despite the fact that in the first case the $E_1$ subband lies in the energy region where also $\Delta_2$ states are present, while in wide MQWs the $E_1$ level is well below the $\Delta_2$ energy edge. Therefore, to simulate the ISB relaxation dynamics we disregard the presence of the $\Delta_2$ states and consider only the coupling between $E_0$ and $E_1$ electrons induced by the phonon and radiation fields.

Following Ref. 7 we assume that a single Fermi distribution with one electron temperature $T_E$ and chemical potential $\mu$ describes the electronic thermal distribution in the two subbands. Monte Carlo calculations show that this is a good approximation for times a few ps after the excitation.[8] As a matter of fact for carrier densities of the order of $10^{11}$ cm$^{-2}$, such as those of our samples, fast elastic scattering processes such as electron-electron and ionized impurity scattering drive the electron gas at the $L$ point to thermalization on a subpicosecond scale.[8] Other elastic scattering mechanisms, for instance interface roughness, may also contribute to the thermalization of the electron gas. The temporal evolution of the electron gas energy (per unit of area and per well), $E_{\rm tot}$, is essentially governed by the coupling of the electronic states with the electromagnetic field and the phonon bath, and can be obtained from the rate equation

$$\frac{dE_{\rm tot}}{dt} = \hbar\omega_{\rm pump} W_g - P_{OP} - P_{AC}. \qquad (1)$$

In the above equation $W_g$ is the net photon absorption rate resulting from the absorption and stimulated emission due to the incident radiation of the pump beam with energy $\hbar\omega_{\rm pump}$, and $P_{OP}$ and $P_{AC}$ are the net energy-loss rates related to the absorption and emission of optical and acoustic phonons, respectively. Note that the terms on the right-hand side of Eq. (1) depend on the electron temperature $T_E$ and chemical potential $\mu$. The temporal evolution of $T_E$ and $\mu$ is obtained by simultaneously solving the equations

$$\sum_{i=0,1} \int_{E_i}^{\infty} \frac{D(E-E_0)dE}{1+e^{(E-\mu)/k_BT_E}} = E_{\rm tot} \quad \text{and} \quad N_0(t) + N_1(t) = N_{\rm tot}, \qquad (2)$$

where $N_0(t)$ [$N_1(t)$] is the 2D carrier density in the lower [upper] confined subband at time $t$ after the pump excitation, $N_{\rm tot}$ is the total equilibrium carrier density per well (i.e., as obtained in the absence of optical excitation solving the

Schrödinger-Poisson equations with $T_E$ equal to the lattice temperature $T_L$), $D = \frac{4m_d}{\pi\hbar^2}$ is the density of states per unit area for the four degenerate $L$ valleys, and $m_d$ is the density-of-state mass at $L$. Finally, $E_i$ are the subband minima with the zero of energy set at the bottom of the ground subband at $L$.

For the description of the temporal profile of the beam intensity $I(t)$ incident on the sample, we use Gaussian lineshapes centered at $t = 0$ whose energy-dependent durations are chosen to reproduce the bandwidth-limited Gaussian pulses of the FELBE. Typical values of the FWHM are 13 (5) ps for the beam energy of 14 (29) meV used in Ref. 14 with the sample S1745 (S1776). Finally, we assume that the pulse intensity in the MQW region $\bar{I}(t)$ remains spatially uniform in the $z$ direction because the shortest wavelength employed is $\gtrsim 10\,\mu$m (inside the semiconductor), which is much larger than the MQW region thickness. We also estimate that the pulse intensity $\bar{I}(t)$ is reduced to about 20% of its value outside the sample $I(t)$ because of reflection losses [the transverse magnetic (TM) reflection coefficient is 0.36] and geometrical mismatch between the circular laser spot and the rectangular sample section.

Most importantly for the results presented in this work, the time-dependent carrier densities $N_0(t)$ and $N_1(t)$ deeply influence the energy of the optical absorption resonance $\tilde{E}_{01}$. In fact, because of the depolarization shift effect[15] $\tilde{E}_{01}$ occurs at higher energies with respect to the bare transition energy $E_{01} = E_1 - E_0$. Since this effect is governed by the carrier densities in the two levels considered, it follows that, under nonequilibrium conditions, the magnitude of the depolarization shift varies dynamically during the relaxation process. In fact the absorption energy resonance obeys the relation[15,21]

$$\tilde{E}_{01}^2(t) = E_{01}^2(1+\alpha(t)), \quad \alpha(t) = \frac{2e^2 S}{\epsilon\epsilon_0 E_{01}}[N_0(t) - N_1(t)], \tag{3}$$

where $S$ is an effective length which is determined from the envelope wave functions $\psi_0$ and $\psi_1$ as

$$S = \int_{-\infty}^{+\infty} dz \left[\int_{-\infty}^{z} dz' \psi_1(z')\psi_0(z')\right]^2. \tag{4}$$

From the above equations it is apparent that the time dependence of $\alpha(t)$ is controlled by the difference of the 2D carrier densities in the $E_0$ and $E_1$ subbands.

The generation rate $W_g$ of Eq. (1) can be written as

$$W_g = \sigma(t)\bar{I}(t)[N_0(t) - N_1(t)]/\cos\theta, \tag{5}$$

where $\sigma(t)$ is the time-dependent absorption cross section evaluated at $\hbar\omega_{\text{pump}}$ and $\theta$ is the propagation angle with respect to the growth direction of the pump pulse in the MQW region, calculated taking into account the facet orientation, and the refractions at the air/facet and at the wafer/MQW interfaces. For the experiments of Ref. 14 we get $\theta \simeq 56^\circ$. The absorption cross section $\sigma(t)$ is

$$\sigma(t) = \frac{e^2\pi\hbar}{2\epsilon_0 c n m_0} \frac{(\Gamma/\pi)2\tilde{E}_{01}(t)2\hbar\omega_{\text{pump}}}{[\tilde{E}_{01}(t)^2 - (\hbar\omega_{\text{pump}})^2 + \Gamma^2]^2 + (2\hbar\omega_{\text{pump}}\Gamma)^2} \times \sum_\gamma f_{01}^\gamma. \tag{6}$$

The sum of the oscillator strengths $f_{01}^\gamma$ is over the four degenerate $L$ valleys and is calculated according to[22]

$$f_{01}^\gamma = \frac{2m_0}{E_{01}}\left(\hat{e}_x w_{xz}^\gamma + \hat{e}_y w_{yz}^\gamma + \hat{e}_z w_{zz}^\gamma\right)^2 \left|p_{01}^z\right|^2, \tag{7}$$

where the growth direction is chosen along the $z$ axis, $w_{ij}^\gamma$ are the components of the inverse mass tensor in the $\gamma$ valley, and $\hat{e}$ is the polarization vector of the TM mode in the MQW region. In Eq. (6) the ISB absorption lineshape is described with a Lorentizian broadening, and for the HWHM we chose, in agreement with the experimental values reported in Ref. 14, the value $\Gamma = 1.7$ (3) meV for the samples with (without) the undoped spacer.

The temporal evolutions of the carrier population and of the absorption cross section are the essential ingredients to calculate the relative differential transmission signal $\frac{\Delta T(t)}{T(t=-\infty)}$ across the $N_{QW} = 20$ stack of MQWs, which is the physical quantity measured in the experiments. At the probe frequency $\omega_{\text{probe}} = \omega_{\text{pump}}$, $\frac{\Delta T(t)}{T(t=-\infty)}$ is given by

$$\frac{\Delta T(t)}{T(t=-\infty)} = 1 - \left[\frac{e^{\sigma(t)[N_0(t)-N_1(t)]}}{e^{\sigma(-\infty)[N_0(-\infty)-N_1(-\infty)]}}\right]^{\frac{N_{QW}}{\cos\theta}}. \tag{8}$$

The net energy-loss rates $P_{OP}$ in Eq. (1) describe the interaction with the optical phonon bath. In covalent crystals the electron-phonon interaction is mediated only by the deformation potential, and, if dispersionless phonon branches are assumed, $P_{OP}$ can be calculated analytically since the electron-phonon coupling does not depend on the phonon momentum, as happens instead for the case of III-V materials, where the coupling is inversely proportional to the modulus of the momentum. Intra- and interband scattering processes are treated separately, using two different effective deformation potentials $\Xi_{OP}$ and phonon energies $\hbar\omega_{\text{eff}}$. The values, taken from Ref. 23, are $\Xi_{OP} = 3.5$ (5.26) $10^8$ eV/cm and $\hbar\omega_{\text{eff}} = 37$ (24) meV for intra- (inter-) valley events, respectively. We start from the probability per unit time $W_{if}^{\mp}(k_i)$ for an electron in subband $i = 0,1$ and in-plane momentum $k_i$ to be scattered in subband $f = 0,1$ by phonon absorption or emission. Treating the lattice excitations as bulk 3D phonons one obtains[24]

$$W_{if}^{\mp}(k_i) = \Theta\left(k_{f\pm}^2\right)\frac{n_{\text{dest}} m_d \Xi_{OP}^2}{2\hbar^2\rho\omega_{\text{eff}}}\left[N(\omega_{\text{eff}},T_L) + \frac{1}{2} \mp \frac{1}{2}\right] \times F_{if}[1 - f(E_f,k_f^{\pm},T_E,\mu)], \tag{9}$$

where $n_{\text{dest}} = 1$ ($n_{\text{dest}} = 3$) is the number of destination valleys involved in intra- (inter-) valley scattering events, $\rho$ is the Ge mass density, $N(\omega_{\text{eff}},T_l)$ is the phonon population at lattice temperature $T_L$, and $f(E_f,k_f^{\pm},T_E,\mu)$ is the Fermi-Dirac distribution for electrons in subband $f$ and in-plane momentum $k_f^{\pm}$ at electron temperature $T_E$. In the above equation and in the following, the upper (lower) sign of $\pm$ and $\mp$ indicates absorption (emission) of a phonon. The value of $k_f^{\pm}$ follows from energy conservation and is given by

$$\frac{\hbar^2 k_i^2}{2m_\parallel} + E_i \pm \hbar\omega_q = \frac{\hbar^2 (k_f^{\pm})^2}{2m_\parallel} + E_{f.} \tag{10}$$

The Heaviside function $\Theta$ in Eq. (9) ensures that the final states for which the energy is conserved belong to the subband $f$.

Finally, in Eq. (9) $F_{if}$ is equal to

$$F_{if} = \int dz \psi_f^2(z)\psi_i^2(z). \tag{11}$$

$P_{OP}$ is evaluated considering all the different scattering channels,

$$P_{OP} = \sum_{i,f}\sum_{k_i} \hbar\omega_{\rm eff}(W_{if}^+(k_i) - W_{if}^-(k_i)) f(E_i,k_i,T_E,\mu)$$
$$\equiv \sum_{i,f} \hbar\omega_{\rm eff}(W_{if}^+ - W_{if}^-), \tag{12}$$

where summation over both inter- and intrasubband scattering channels is understood. The sum over $k_i$ is converted into an energy integral which can be evaluated analytically. The resulting expression for $W_{if}^{\mp}$ is

$$W_{if}^{\mp} = D^2 \frac{n_{\rm dest}\pi\hbar\Xi_{OP}^2}{8\rho\hbar\omega_{\rm eff}} F_{if}\left[N(\omega_{\rm eff},T_L) + \frac{1}{2} \mp \frac{1}{2}\right] Z \tag{13}$$

where

$$Z = k_B T_E \frac{b}{b-1}\ln\left(1 + \frac{b-1}{1+ab}\right) \tag{14}$$

and

$$a = \exp\left[\frac{\max(E_f \mp \hbar\omega_{\rm eff}, E_i) - \mu}{k_B T_E}\right], \quad b = e^{\pm\hbar\omega_{\rm eff}/k_B T_E}. \tag{15}$$

Differently from $P_{OP}$, the net energy loss rate $P_{AC}$ related to the interaction of the $E_0$ and $E_1$ electrons with the 3D acoustic phonon bath cannot be treated analytically. This fact is due to the nonrigid momentum conservation in the direction perpendicular to the layer planes. Indeed, in order to calculate $P_{AC}$ at each time step of the discretized version of Eq. (1), the nonvanishing dispersion of the acoustic branch makes the numerical evaluation of a triple integral unavoidable.[25–27] However, such computational load can be avoided if, following Ref. 7, an approximate relation is adopted. To justify this point one can verify that when the subband separation is below the optical phonon energy, $P_{AC}$ is comparable with $P_{OP}$ only at low electron temperatures, where optical phonon scattering is suppressed by energy conservation and the majority of the carriers are already relaxed in the $E_0$ subband. It follows that in this regime the energy loss mechanism which dominates $P_{AC}$ is the intrasubband electron cooling in the first subband. Therefore we evaluate $P_{AC}$ relying on a semiempirical expression for the 2D intrasubband acoustic scattering, first proposed in Ref. 28 and often adopted in the literature (see for instance Refs. 7 and 29). This relation has been derived to reproduce and interpolate the analytical results which can be obtained in the high (equipartition) and low $T_L$ (Bloch-Gruneisen) regimes, where $P_{AC}$ is proportional to $T_E - T_L$ and $T_E^5 - T_L^5$, respectively. The expressions, adopted from Ref. 28 and modified to normalize to surface unit and take into account the presence of four degenerate $L$ valleys, are

$$P_{AC} = FC_{np}(T_E - T_L), \quad C_{np} = \frac{3\pi k_B \hbar \Xi_{AC}^2 D^2 N_0}{64\rho k_f}, \tag{16}$$

where $k_f$ is the Fermi wave vector, $\Xi_{AC} = 2.5$ eV is the acoustic deformation potential of Ge whose value is taken from Ref. 23, and

$$F = \frac{\sinh(x_L - x_E)}{\sinh x_L \sinh x_E}\left(\frac{x_E x_L}{x_L - x_E}\right), \quad x_{E,L} = \frac{\hbar\omega_{\rm avg}}{2k_B T_{E,L}}, \tag{17}$$

where $\hbar\omega_{\rm avg} = \sqrt{2}\hbar v_s k_f$ and $v_s$ is the Ge sound velocity.

## III. RESULTS FOR THE RELAXATION DYNAMICS

To get a first insight into the ISB relaxation dynamics we report in Fig. 2 the temporal evolution of some relevant physical quantities, calculated for the sample S1745 at $T_L = 4$ K, with $I_{\rm max} = I(t=0)$ equal to $2\times10^3$ and $5\times10^2$ W/cm$^2$. The resulting relaxation processes for these two pump powers are quite different. In fact the higher beam intensity heats the electron gas up to about 50 K while at the lower beam intensity the electron temperature is $T_E \lesssim 20$ K. Consequently, only in the former case is there a significant fraction of carriers in the $E_1$ subband. This fact is also suggested by the temporal

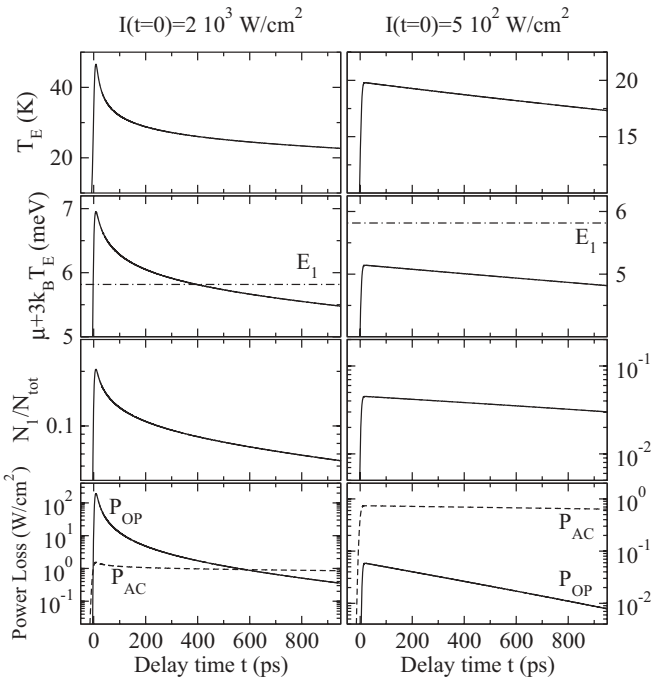


FIG. 2. Relaxation of relevant physical variables for the sample S1745 at lattice temperature $T_L = 4$ K, calculated as a function of the probe time delay $t$ and for the maximum intensity of the single pulse of the pump beam (outside the sample) $I(t=0) = 2\times10^3$ W/cm$^2$ (left plots) and $I(t=0) = 5\times10^2$ W/cm$^2$ (right plots). As in Ref. 14 the HWHM of the ISB absorption resonance is 3 meV and the pump energy is detuned toward the red by 2.1 meV. From top to bottom, the electron temperature $T_E$, $\mu + 3k_B T_e$ together with the bottom energy of the $E_1$ subband, the fraction of electrons in the $E_1$ subband $N_1/N_{\rm tot}$, and the total optical and acoustic power-loss rates $P_{OP}$ and $P_{AC}$ in the $N_{QW} = 20$ QWs, are reported. The fast relaxation dynamics present in the left plots (higher pump intensity) soon after excitation is due to optical phonon emission. An exponential fit of the $N_1/N_{\rm tot}$ curve in this time region in the left (right) plot gives for the relaxation time the value $\tau \simeq 90$ (2400) ps. Note that the scale of the vertical axis in the left and right plots is not the same.

evolution of the chemical potential $\mu$, which always remains more than $3k_BT_E$ below the bottom of the $E_1$ subband when the system is pumped with the lower intensity beam (see Fig. 2). Due to the pump-induced electron heating, soon after the excitation some of the $E_1$ carriers have sufficient kinetic energy to relax into the $E_0$ subband via optical phonon emission. If $T_E$ is large enough, this mechanism dominates over the $P_{AC}$ term, as shown in the bottom-left plot of Fig. 2 for $t \lesssim 550$ ps. For larger delay times $T_E$ reduces and the optical phonon emission quenches since the kinetic energy of the electronic population in the $E_1$ subband diminishes and the intersubband spacing is lower than the optical phonon energy. Acoustic intersubband cooling in the $E_0$ subband becomes then the dominant energy relaxation mechanism of the electron gas.

It follows that, similarly to what is observed in the case of large GaAs/AlGaAs MQWs,[7] at high pumping intensities a double exponential behavior is obtained for $N_1(t)/N_{\rm tot}$, with a transition from an initial fast relaxation rate, where optical phonon emission dominates, to a slower one, controlled by $E_0$ intrasubband cooling via acoustic phonon emission. The two related relaxation times $\tau$ calculated for the case of Fig. 2 (left plots) are ~90 ps and 2400 ps, respectively. We find that these quantities strongly depend on $I_{\rm max}$ which controls the zero-delay value of $T_E$. For instance, increasing the pump intensity to $\sim 10^4$ W/cm$^{-2}$, the maximum of $N_1(t)/N_{\rm tot}$ approaches the 50% saturation value for which $W_g(t) = 0$ (transparency condition) and the initial relaxation time diminishes from 90 ps to about 25 ps. We stress that this quantity is in very good agreement with the value of 27 ps measured in Ref. 14 for the sample S1745 with pump intensity in the QW region of about $6 \times 10^3$ W/cm$^{-2}$. In agreement with the theoretical model, in the same sample also the double exponential behavior with a fast initial relaxation time and a successive much slower exponential tail has been experimentally obtained; this is shown in the top panel of Fig. 4 where the measured $\Delta T(t)/T$ signal is reported.

As already pointed out, the transition from an initial fast relaxation rate, where optical phonon emission dominates, to a slower one, controlled by $E_0$ intrasubband cooling via acoustic phonon emission, takes place when the electron gas reach the crossover electron temperature $T_{co}$ for which the $P_{OP}$ power-loss term starts to dominate the $P_{AC}$ power-loss term. The authors of Ref. 7 used pump-probe experiments in conjunction with an energy relaxation model to estimate $T_{co}$ in two GaAs/AlGaAs MQWs samples, for which the $E_0 \rightarrow E_1$ transition energies (at 19 and 27 meV, corrected by the depolarization shift) are lower than the optical phonon energy (37 meV) and the carrier densities ($2 \times 10^{11}$ cm$^{-2}$) are comparable to the corresponding quantities of the systems addressed in this work. They found that, for low lattice temperature, the crossover electron temperature $T_{co}$ is about 35 K. It is interesting to compare this value with the ones estimated for the Ge/SiGe MQW systems here studied. To this aim we report in the top panel of Fig. 3 the $P_{AC}$ and $P_{OP}$ terms calculated for the sample S1776 ($\tilde{E}_{01} = 32$ meV, $N_{\rm tot} = 3 \times 10^{11}$ cm$^{-2}$) and the sample S1750 ($\tilde{E}_{01} = 13$ meV, $N_{\rm tot} = 3 \times 10^{11}$ cm$^{-2}$) as a function of the electron temperature, at $T_L = 4$ K. We find for both samples $T_{co} \simeq 25$ K. This value is similar to the one obtained for the GaAs/AlGaAs MQW systems, despite the absence of the polar optical phonon coupling in group IV structures, which is instead the dominant phonon scattering mechanism in III-V based systems. The similarity of the $T_{co}$ values might be attributed to a larger power loss in GaAs/AlGaAs MQWs related also to the interaction with acoustic phonons. In fact the acoustic deformation potential of GaAs ($\Xi_{AC} = 7$ eV, see Ref. 29) is about three times the value measured in Ge. Moreover in III-V materials there is also a contribution to the acoustic phonon power loss stemming from the polar interactions.[25] We notice, however, that a more quantitative comparison between acoustic and optical phonon power-loss rates in Ge/SiGe and GaAs/AlGaAs MQWs is quite demanding and beyond the scope of the present work. Indeed, toward this aim one should consider also the effects arising from the very different electronic band structures of these two materials. For instance, at equal carrier density, the fourfold

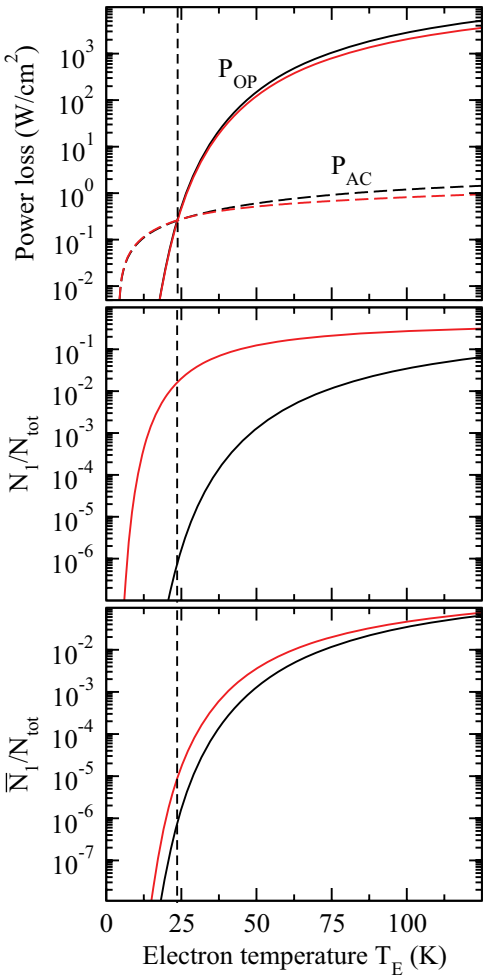


FIG. 3. (Color online) Power losses and carrier densities for the samples S1776 (black curves) and S1750 (red curves), calculated as a function of the electron temperature and for lattice temperature $T_L = 4$ K. Power losses due to the interaction with acoustic (dashed lines) and optical (solid lines) phonons are reported in the top panel and refer to $N_{QW} = 20$ quantum wells. The fraction of carriers in the first excited subband, $N_1/N_{\rm tot}$, is shown in the central panel. The fraction of carriers in the first excited subband whose energy allows intersubband relaxation via optical phonon emission, $\overline{N}_1/N_{\rm tot}$, is shown in the bottom panel. The vertical dashed lines represent the effective optical phonon energy for intervalley scattering.

degeneracy of the lowest conduction valleys in Ge, which instead is absent in GaAs, lowers the position of the Fermi energy and then strongly affects the scattering rates.

At the found value of $T_{co}$ the fraction $N_1/N_{\rm tot}$ is still quite small (about $2 \times 10^{-2}$ and $1 \times 10^{-6}$ for samples S1750 and S1776, respectively) as shown in the central panel of Fig. 3. In fact, in order to relax the electron energy, the optical phonon emission is a much more effective mechanism than the intersubband cooling via acoustic phonon emission. Indeed the fraction of carriers in the first excited subband with enough energy to emit an optical phonon, $\overline{N}_1/N_{\rm tot}$, is even smaller than $N_1/N_{\rm tot}$. $\overline{N}_1/N_{\rm tot}$ is shown in the bottom panel of Fig. 3 as a function of the temperature. For the sample S1750 at $T_{co}$ we estimate that $\overline{N}_1 \simeq 10^{-3} N_1$.

To study the role of the intersubband separation in the relaxation dynamics, the time-dependent relative differential transmissions of samples with different widths $d_{QW}$ have been evaluated. Results for MQW systems with the bare $E_{01}$ energy in the 10–68 meV range with $T_L = 4$ K and $I_{\rm max} = 3 \times 10^4$ W/cm$^2$ are shown in Fig. 4. The pump beam energies $\hbar\omega_{\rm pump}$ were chosen to be resonant with the values of the depolarized absorption resonances $\tilde{E}_{01}$, evaluated in the absence of optical excitation; the pulse widths have been calculated assuming transform limited durations. For this choice of $\hbar\omega_{\rm pump}$, the temporal dependence of $N_1(t)/N_{\rm tot}$ and $\Delta T(t)/T$ are qualitatively similar (detuning effects between $\hbar\omega_{\rm pump}$ and $\tilde{E}_{01}$ are discussed in the next section). As one can expect, we find that with increasing $E_{01}$ the relaxation becomes faster. In fact when $E_{01} > \hbar\omega_{\rm eff}$ all the electrons excited in the $E_1$ subband have enough energy to relax in the $E_0$ subband via emission of optical phonons. On the other hand, for $E_{01} < \hbar\omega_{\rm eff}$, phonon emission is energetically suppressed. In this case, one finds from Eq. (13) that the emission term $W_{10}^{+}$ is proportional to $e^{-\hbar\omega_{\rm eff}/k_B T_E}$ which, for the pump intensities adopted in Fig. 4, is a small quantity. Fitting the $N_1(t)/N_{\rm tot}$ curves soon after excitation with a single exponential, we obtain that when $E_{01}$ increases from 10 to 68 meV the relaxation time drops from about 16 to 0.5 ps (we stress that for large $E_{01}$ values the relaxation time is smaller than the pulse duration, so it does not represent the time scale of the nonradiative component of the ISB dynamics). The variation of $E_{01}$ greatly influences also the amount of excited carriers in the $E_1$ subband and then the value of the relative differential transmission. We observe that the peak values of the $N_1(t)/N_{\rm tot}$ and $\Delta T(t)/T$ curves decrease by more than two and three orders of magnitude respectively when $E_{01}$ is varied from 10 to 68 meV. Of course this effect is to be attributed to the enhancement of the $P_{OP}$ term in Eq. (1) while variations in the pump term $\hbar\omega_{\rm pump} W_g(t)$ of Eq. (1) play a negligible role. At the chosen pump intensity, the relaxation dynamics shown in Fig. 4 is always driven by $P_{OP}$, which dominates $P_{AC}$ also in the largest MQW system. Indeed as shown in Fig. 5, the peak electron temperature $T_E^{\rm max}$ after optical excitation is well above the $T_{co}$ value. To get a deeper insight into the dependence of the relaxation dynamics on transition energies, we report in Fig. 5 also the peak value for the relative density of those carriers in the $E_1$ subband whose energy is sufficient to emit optical phonons in intersubband scattering events ($\overline{N}_1/N_{\rm tot}$). Note that while the peak value of $N_1/N_{\rm tot}$ monotonically decreases for increasing $E_{01}$ (see

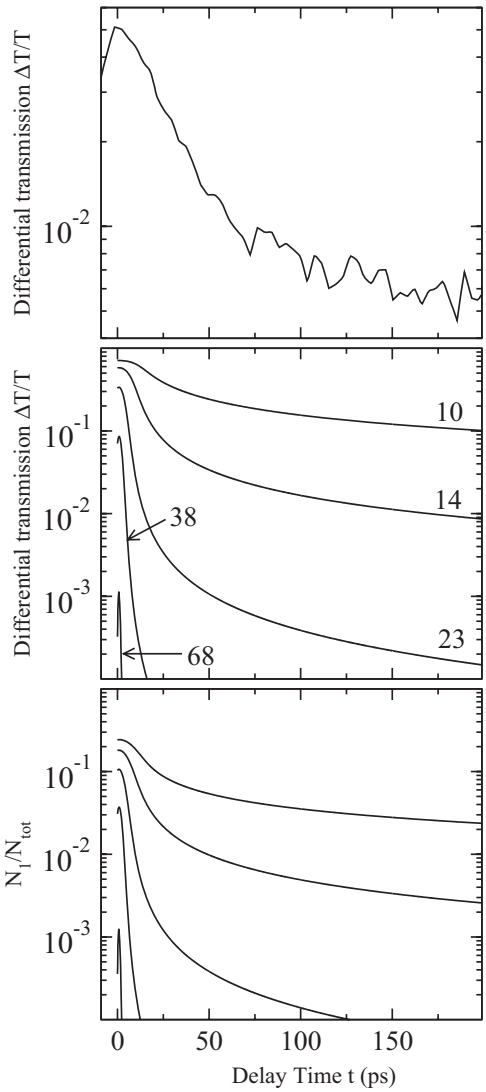


FIG. 4. Top panel: Time-resolved relative differential transmission measured at FELBE on sample S1745 with absorption energy at equilibrium $\tilde{E}_{01} = 16$ meV. The fast (slow) exponential relaxation time is 34 (194) ps. Central and bottom panels: Calculated relative carrier population in the $E_1$ subband and transmission change as function of the probe time delay, at $T_L = 4$ K for different QW widths in the 70–230 Å range; the respective $E_{01}$ bare transition energies are reported in meV in the central panel. An undoped barrier region of 100 Å is present on each side of the Ge QW layer. The 2D charge carrier densities $N_{\rm tot}$ vary in the 1–3 $\times 10^{11}$ cm$^{-2}$ interval. The pump energies are resonant with the depolarized $\tilde{E}_{01}$ absorption energies calculated in the absence of optical excitation. The maximum pump intensity outside the sample is fixed at $I(t=0) = 3 \times 10^4$ W/cm$^2$. Increasing $d_{QW}$, the FWHM of the beam pulse varies from 2 to 11 ps.

Fig. 4), both $\overline{N}_1/N_{\rm tot}$ and $T_E^{\rm max}$, calculated as function of $E_{01}$, have a maximum in the investigated energy range. To account for this nonmonotonic behavior, we note that, for transition energies above the optical branch, optical phonon emission is not suppressed, i.e., $W_{OP}$ is large and then the majority of carriers remains in the $E_0$ subband. As a consequence small values of $\overline{N}_1/N_{\rm tot} = N_1/N_{\rm tot}$ are obtained in this energy region. On the other hand, for small transition energies, a larger fraction of carriers is excited in the $E_1$ subband. However,

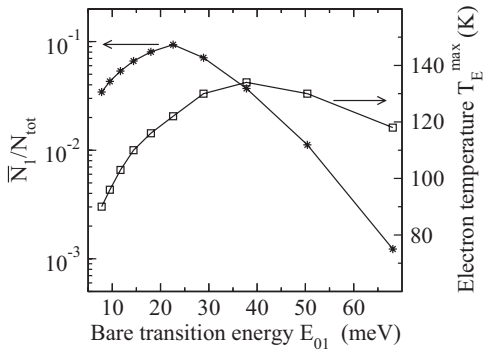


FIG. 5. Peak values after resonant optical excitation of the electron temperature (right vertical axis) and of the population fraction $\overline{N}_1/N_{tot}$ of the carriers in the $E_1$ subband whose energy allows emission of optical phonons (left vertical axis), shown as function of the $E_{01}$ bare transition energy. Data have been obtained using the same parameters as in Fig. 4.

due to the small subband separation, only few of them have enough energy to emit optical phonons. It follows that the ratio $\overline{N}_1/N_{tot}$ is small also for transition energies well below the optical phonon energy. As a consequence a maximum for $\overline{N}_1/N_{tot}$ as a function of the transition energy is obtained at $E_{01} \simeq 22$ meV.

As already anticipated we obtain a good agreement between calculated and measured relaxation times, which fall in the range 25–35 ps. This is especially true for large well widths and low lattice temperatures (e.g., samples S1745 and S1750 in Ref. 14). This fact may be taken as a validation of the model, and of the adopted parameters. The dependence of the relaxation time on $E_{01}$ presented in Fig. 4 has not been observed in the experiment of Ref. 14, where fast exponential decays with $\tau$ values around 30 ps were observed for all the investigated samples with $E_{01}$ ranging from 15 to 28 meV. Possibly, the deviation from the Gaussian time profile of real pulses from the free electron laser, whose duration can be longer than the Fourier-transform-limited value, may have hindered the observation of fast relaxation phenomena in the first few tens of ps delays. Moreover, deviations between the theoretical and measured results may also arise from the presence of undoped spacer layers between donors atoms and the wells (as in sample S1776 of Ref. 14) which reduces ionized impurity scattering.[16] As a matter of fact, the ionized impurity scattering is one of the main channels of fast thermalization of carriers within the subbands, which is the main hypothesis behind our model. Possibly, the presence of spacer layers in S1776 did not allow electron thermalization within tens of ps, and the relative differential transmission soon after optical excitation might be controlled by the elastic scattering time, and not by phonons as suggested in Ref. 14.

## IV. DYNAMICAL DEPOLARIZATION SHIFT

We now discuss the effects in the relative differential transmission spectra related to the pump-probe energy detuning

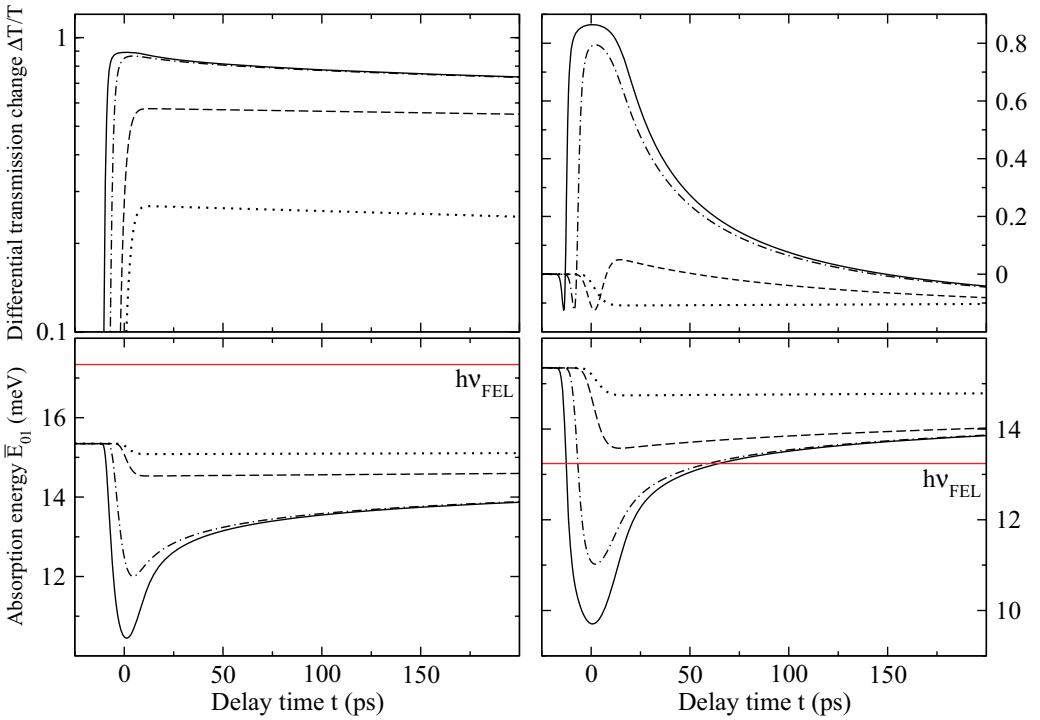


FIG. 6. (Color online) Relative differential transmission (top panels) and depolarized $\tilde{E}_{01}$ intersubband absorption energy (bottom panels) as a function of probe delay calculated for the sample S1745. In the left (right) panels the pump and probe beam energy represented by the red horizontal line is set 2 meV above (below) the equilibrium value of $\tilde{E}_{01}$. The HWHM of the absorption resonance is set to 3 meV and the peak pulse intensities are $5 \times 10^2$ (solid), $1 \times 10^3$ (dashed), $1 \times 10^4$ (dot-dashed), and $1 \times 10^5$ W/cm$^2$ (dotted). The 2D carrier density per well is $7 \times 10^{11}$ cm$^{-2}$.

with respect to the ISB depolarized absorption resonance energy $\tilde{E}_{01}$. As already mentioned when discussing Fig. 4, if $\hbar\omega_{\text{pump}}$ is resonant with the equilibrium value of the depolarized absorption energy $\tilde{E}_{01}$, positive $\Delta T/T$ signals (bleaching) are found. Correspondingly, the decay of the relative differential transmission signal is qualitatively similar to the temporal evolution of $N_1/N_{\text{tot}}$. The same holds when the pump beam energy is set above the absorption resonance (see top-left panel in Fig. 6). In contrast, we predict qualitatively different behaviors for $\Delta T/T$ (including negative relative differential transmission signals) if $\hbar\omega_{\text{pump}}$ is at a (slightly) lower energy with respect to the equilibrium value of the $\tilde{E}_{01}$ absorption resonance. This effect is shown in the top-right panel of Fig. 6, where $\Delta T/T$ is plotted for different excitation intensities with $\hbar\omega_{\text{pump}}$ set 2 meV below $\tilde{E}_{01}$. We see that, at the smallest pump beam intensity (solid line), $\Delta T/T$ is always negative. For higher intensities, the signal is initially negative, while positive values are found only at later times. The observed effect can be understood by considering the depolarization effect, which dynamically shifts the absorption resonance as described in Eq. (3) and shown graphically in the bottom panels of Fig. 6. Indeed, when carriers are promoted in the $E_1$ subband, $\tilde{E}_{01}$ red-shifts, since the excess of carrier density $N_1(t)$ is responsible for a decrease of $\alpha(t)$ [see Eq. (3)]. Then, if $\hbar\omega_{\text{pump}}$ is above the equilibrium value of $\tilde{E}_{01}$ as in the case shown in the left panels of Fig. 6, for the absorption cross section evaluated for $\hbar\omega_{\text{probe}} = \hbar\omega_{\text{pump}}$ at positive delay times $t$, it holds that $\sigma(t) < \sigma(-\infty)$. The reduced cross section is therefore responsible for higher transmission of the probe light. This fact enhances the bleaching effect related to the population dynamics [see Eq. (8)] and then positive values of the relative differential transmission signal are obtained. On the other hand, when $\hbar\omega_{\text{pump}}$ is below the equilibrium value of $\tilde{E}_{01}$, the dynamical redshift of the absorption resonance may tune the peak absorption to the photon beam energy and thus increase the cross section. Then, despite the presence of an excess of carriers in the $E_1$ subband, from Eq. (8) it follows that negative relative differential transmission signals occur if $\sigma(t)[N_0(t) - N_1(t)] > \sigma(-\infty)[N_0(-\infty) - N_1(-\infty)]$.

We now provide a validation of the dynamical depolarization shift effects predicted by the model, through direct comparison of the calculated relative differential transmission signals with experimental data collected at FELBE. In Fig. 7 we show the measured and calculated relative differential transmission $\Delta T/T$ as a function of probe delay time for the sample S1745 ($d_{QW} = 24$ nm). This sample, among all the samples analyzed in Ref. 14, displays the highest electron density and hence, according to Eq. (3), the strongest relative magnitude of the depolarization shift effect if compared with the bare $E_{01}$ transition energy. The probe beam energy of 14.1 meV is just below the experimental low-temperature equilibrium value of the ISB absorption resonance, measured by means of Fourier transmission spectroscopy at 16.2 meV. In the measurement, the photon flux of the pump pulse was well above the total electron density present in the wells, leading to saturation of the $E_0 \rightarrow E_1$ transition and consequently of the relative differential transmission signal. Setting the $I(t = 0)$ value in this saturation region so as to reproduce the peak intensity of the measured $\Delta T/T$ signal, we obtain

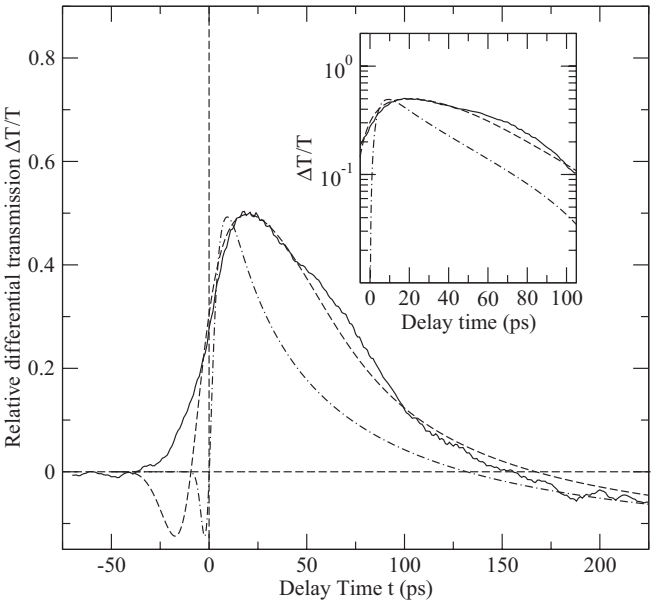


FIG. 7. Relative differential transmission for the sample S1745 at $T_L = 4$ K. The solid curve represents the experimental data obtained with the pump-probe beam redshifted by 2.1 meV with respect to the $\tilde{E}_{01}$ resonance. The other curves are the numerical data for $\Delta T/T$, obtained with transform limited pulse beam duration (dashed line) and with a Gaussian pump beam whose (larger) duration has been used as a fitting parameter (dot-dashed line). In the inset, the same curves are reported on a vertical logarithmic scale. The change of sign of $\Delta T/T$ from positive to negative is a signature of the dynamical depolarization shift effect discussed in the text.

the numerical results reported in Fig. 7. The dot-dashed curve shown in Fig. 7 has been obtained by imposing a Fourier-transform-limited pulse duration. Note that in this case the rise of the $\Delta T/T$ signal at zero delay is steeper than the measured one. This may be attributed to deviations from the Gaussian lineshape in the real pulse. To take into account this effect we have performed simulations with a pulse duration longer than the Fourier-transform limit. The duration value was instead chosen to fit the measured $\Delta T/T$ signal just before $t = 0$ (dashed curve in Fig. 7). In this case a much better agreement with the experimental data is obtained, also for longer delay times. In the time delay window below 80 ps, both calculated and measured curves display a similar time dependence with a weak deviation from a pure exponential behavior, as evidenced in the inset of Fig. 7. More importantly, for time delays above 100 ps, $\Delta T/T$ strongly deviates from a single exponential decay regime, and changes its sign from positive (bleaching) to negative (pump-induced absorption), as predicted by the dynamical depolarization shift model discussed above. Note that not only the qualitative change of sign of $\Delta T/T$ is reproduced by the model, but also the time delay for which the change of sign occurs ($t \simeq 150$ ps). We stress that the accurate prediction of the point of sign inversion is a strong evidence of the validity of the model, since it is quite independent from both the laser pulse duration and the pump intensity $I(t = 0)$, whose experimental values are not known with high accuracy.

## V. CONCLUSIONS

We have theoretically and numerically investigated the nonradiative intersubband relaxation dynamics in $n$-type Ge/SiGe MQW systems with high carrier density and intersubband transitions in the terahertz range, below the Ge-optical phonon energy (37 meV).

We have introduced an energy balance model to describe the time-resolved relaxation of Ge/SiGe MQW systems after optical excitation, resonant with the ISB transition. Interaction of the electron system with both the optical and acoustic phonon baths and the radiation field is evaluated as a function of the probe delay time. A crossover electron temperature above which optical phonon emission becomes dominant, even for energy spacing well below 37 meV, is defined. The time-resolved relative differential transmission has been numerically evaluated under different experimental conditions such as Ge well width, pump intensity, and photon energy.

The model also describes the dynamical variation of the intersubband absorption energy, which is caused by the change of the electron population in the $E_0$ and $E_1$ subbands after absorption of pump photons. Indeed we have shown that the magnitude of the depolarization shift of the ISB absorption energy is a dynamical quantity, changing instantaneously during the much slower time scale of the nonradiative ISB relaxation (tens to hundreds of ps). This fact may have a profound effect on the differential transmission signal, which can be enhanced, suppressed, or can even change its sign.

Numerical simulations have been compared to relative differential transmission signals measured at FELBE on a series of Ge/SiGe MQW samples. A nice agreement with the measured fast initial relaxation times around 30 ps, due to nonpolar optical phonon emission, is obtained. The observed residual relaxation with longer characteristic time is reproduced by the model and attributed to intersubband cooling in the lowest subband via acoustic phonon emission. Clear signatures of the dynamical depolarization shift effect have been highlighted in the experimental data.

## ACKNOWLEDGMENTS

The authors gratefully acknowledge Manfred Helm for stimulating discussions. This work was partly supported by the European Community Seventh Framework Programme under grant agreement No. 226716. One of the author (M.O.) was supported by the Italian Ministry of Research through Grant No. FIRB-RBFR08N9L9.

*virgilio@df.unipi.it

[1] C. Gmachl, F. Capasso, D. L. Sivco, and A. Y. Cho, Rep. Prog. Phys. **64**, 1533 (2001).

[2] F. Giorgetta, E. Baumann, M. Graf, Q. Yang, C. Manz, K. Kohler, H. Beere, D. Ritchie, E. Linfield, A. Davies, Y. Fedoryshyn, H. Jackel, M. Fischer, J. Faist, and D. Hofstetter, IEEE J. Quantum Electron. **45**, 1039 (2009).

[3] J. A. Levenson, G. Dolique, J. L. Oudar, and I. Abram, Phys. Rev. B **41**, 3688 (1990).

[4] J. Faist, F. Capasso, C. Sirtori, D. L. Sivco, A. L. Hutchinson, S. N. G. Chu, and A. Y. Cho, Appl. Phys. Lett. **63**, 1354 (1993).

[5] D. Y. Oberli, D. R. Wake, M. V. Klein, J. Klem, T. Henderson, and H. Morkoç, Phys. Rev. Lett. **59**, 696 (1987).

[6] B. N. Murdin, G. M. H. Knippels, A. F. G. van der Meer, C. R. Pidgeon, C. J. G. M. Langerak, M. Helm, W. Heiss, K. Unterrainer, E. Gornik, K. K. Geerinck, N. J. Hovenier, and W. T. Wenckebach, Semicond. Sci. Technol. **9**, 1554 (1994).

[7] B. N. Murdin, W. Heiss, C. J. G. M. Langerak, S.-C. Lee, I. Galbraith, G. Strasser, E. Gornik, M. Helm, and C. R. Pidgeon, Phys. Rev. B **55**, 5171 (1997).

[8] M. Dür, S. M. Goodnick, and P. Lugli, Phys. Rev. B **54**, 17794 (1996).

[9] P. Murzyn, C. R. Pidgeon, J.-P. R. Wells, I. V. Bradley, Z. Ikonic, R. W. Kelsall, P. Harrison, S. A. Lynch, D. J. Paul, D. D. Arnone, D. J. Robbins, D. Norris, and A. G. Cullis, Appl. Phys. Lett. **80**, 1456 (2002).

[10] R. W. Kelsall, Z. Ikonic, P. Murzyn, C. R. Pidgeon, P. J. Phillips, D. Carder, P. Harrison, S. A. Lynch, P. Townsend, D. J. Paul, S. L. Liew, D. J. Norris, and A. G. Cullis, Phys. Rev. B **71**, 115326 (2005).

[11] P. Rauter, T. Fromherz, G. Bauer, N. Q. Vinh, B. N. Murdin, J. P. Phillips, C. R. Pidgeon, L. Diehl, G. Dehlinger, and D. Grützmacher, Appl. Phys. Lett. **89**, 211111 (2006).

[12] P. Rauter, T. Fromherz, C. Falub, D. Grutzmacher, and G. Bauer, Appl. Phys. Lett. **94**, 081115 (2009).

[13] A. Valavanis, L. Lever, C. A. Evans, Z. Ikonić, and R. W. Kelsall, Phys. Rev. B **78**, 035420 (2008).

[14] M. Ortolani, D. Stehr, M. Wagner, M. Helm, G. Pizzi, M. Virgilio, G. Grosso, G. Capellini, and M. D. Seta, Appl. Phys. Lett. **99**, 201101 (2011).

[15] M. Helm, in *Intersubband Transitions in Quantum Wells, Physics and Device Applications I*, Semiconductors and Semimetals, Vol. 62, edited by H. C. Liu and F. Capasso (Academic, New York, 2000), Chap. 1, pp. 1–99.

[16] M. De Seta, G. Capellini, M. Ortolani, M. Virgilio, G. Grosso, G. Nicotra, and P. Zaumseil, Nanotechnology **23**, 465708 (2012).

[17] K. Craig, B. Galdrikian, J. N. Heyman, A. G. Markelz, J. B. Williams, M. S. Sherwin, K. Campman, P. F. Hopkins, and A. C. Gossard, Phys. Rev. Lett. **76**, 2382 (1996).

[18] Y. Busby, M. De Seta, G. Capellini, F. Evangelisti, M. Ortolani, M. Virgilio, G. Grosso, G. Pizzi, P. Calvani, S. Lupi, M. Nardone, G. Nicotra, and C. Spinella, Phys. Rev. B **82**, 205317 (2010).

[19] A. Valavanis, T. V. Dinh, L. J. M. Lever, Z. Ikonić, and R. W. Kelsall, Phys. Rev. B **83**, 195321 (2011).

[20] K. Driscoll and R. Paiella, J. Appl. Phys. **102**, 093103 (2007).

[21] M. Załużny, Phys. Rev. B **47**, 3995 (1993).

[22] S. K. Chun and K. L. Wang, Phys. Rev. B **46**, 7682 (1992).

[23] M. Fischetti, IEEE Trans. Electron Devices **38**, 634 (1991).

[24]M. V. Fischetti and S. E. Laux, Phys. Rev. B **48**, 2244 (1993).
[25]B. K. Ridley, Rep. Prog. Phys. **54**, 169 (1991).
[26]S. J. Manion, M. Artaki, M. A. Emanuel, J. J. Coleman, and K. Hess, Phys. Rev. B **35**, 9203 (1987).
[27]A. J. Vickers, Phys. Rev. B **46**, 13313 (1992).
[28]M. Daniels, B. Ridley, and M. Emeny, in *Hot Carriers in Semiconductors*, special issue of Solid State Electron. **32**, 1207 (1989).
[29]N. Balkan, H. Çelik, A. J. Vickers, and M. Cankurtaran, Phys. Rev. B **52**, 17210 (1995).